Possible Orientation Effects to the Phase Diagram of Fundamental Composite Particles

Kwang-Hua W. Chu

P.O. Box 39, Transfer Centre, Road XiHong, Wulumuqi 830000, PR China

Abstract

We obtain possibly valuable information about the phase diagram of rather dense composite particles at high fermion as well as boson number density but low temperature, which is not accessible to relativistic heavy ion collision experiments. Our calculations could qualitatively measure the number of thermodynamic degrees of freedom at the time at which the matter (produced in heavy ion collisions which might be a deconfined quark-gluon plasma) comes into approximate local thermal equilibrium and begins to behave like a hydrodynamic fluid. Possible observational signatures associated with the theoretically proposed states of matter inside compact stars are discussed as well.

1 Introduction

The only place in the universe where we expect sufficiently high densities and low temperatures is compact stars, also known as 'neutron stars', since it is often assumed that they are made primarily of neutrons (for a recent review, see [1]). A compact star is produced in a supernova. As the outer layers of the star are blown off into space, the core collapses into a very dense object. Neutron stars are among the most fascinating bodies in our Universe. They contain over a solar mass of matter within a radius of $\sim$10 km at densities of the order of 10^{15} g/cc. They probe the properties of cold matter at extremely high densities and have proven to be fantastic test bodies for theories of general relativity. In a broader perspective, neutron stars and heavy-ion collisions provide access to the phase diagram of matter at extreme densities and temperatures, which is basic for understanding the very early Universe and several other astrophysical phenomena.
Astrophysicists distinguish between three different kinds of compact stars. These are white dwarfs, neutron stars, and black holes. The former contain matter in one of the densest forms found in the Universe which, together with the unprecedented progress in observational astronomy, makes such stars superb astrophysical laboratories for a broad range of most striking physical phenomena. These range from nuclear processes on the stellar surface to processes in electron degenerate matter at subnuclear densities to boson condensates and the existence of new states of baryonic matter such as color superconducting quark matter at supernuclear densities. More than that, according to the strange matter hypothesis strange quark matter could be more stable than nuclear matter, in which case neutron stars should be largely composed of pure quark matter possibly enveloped in thin nuclear crusts. Neutron stars and white dwarfs are in hydrostatic equilibrium, so at each point inside the star gravity is balanced by the degenerate particle pressure, as described mathematically by the Tolman-Oppenheimer-Volkoff equation [2].

It is often stressed that there has never been a more exciting time in the overlapping areas of nuclear physics, particle physics, and relativistic astrophysics than today [3]. This comes at a time where new orbiting observatories such as the Hubble Space Telescope, Rossi X-ray Timing Explorer (RXTE), Chandra X-ray satellite, and X-ray Multi Mirror Mission (XMM) have extended our vision tremendously, allowing us to see vistas with an unprecedented clarity and angular resolution that previously were only imagined, enabling astrophysicists for the first time ever to perform detailed studies of large samples of galactic and extragalactic objects. On the Earth, radio telescopes (e.g., Arecibo, Green Bank, Parkes, VLA) and instruments using adaptive optics and other revolutionary techniques have exceeded previous expectations of what can be accomplished from the ground. The gravitational wave detectors LIGO, LISA, VIRGO, and Geo-600 are opening up a window for the detection of gravitational waves emitted from compact stellar objects such as neutron stars and black holes.

Neutron stars are dense, neutron-packed remnants of massive stars that blew apart in supernova explosions [1]. They are typically about twenty kilometers across and spin rapidly, often making several hundred rotations per second. Many neutron stars form radio pulsars, emitting radio waves that appear from the Earth to pulse on and off like a lighthouse beacon as the star rotates at very high speeds. Neutron stars in X-ray binaries accrete material from a companion star and flare to life with a burst of X-rays. Measurements of radio pulsars and neutron stars in X-ray binaries comprise most of the neutron star observations. Improved data on isolated neutron stars (e.g. RX J1856.5-3754, PSR 0205+6449) are now becoming available, and future investigations at gravitational wave observatories such as LIGO and VIRGO will focus on neutron stars as major potential sources of gravitational waves. Depending on star mass and rotational frequency, gravity compresses the matter in the core regions of pulsars up to more than ten times the density of ordinary atomic nuclei, thus providing a high pressure environment in which numerous subatomic particle processes compete with each other.

The most spectacular ones stretch from the generation of hyperons and baryon resonances to quark deconfinement to the formation of boson condensates. There are theoretical suggestions of even more exotic processes inside neutron stars, such as the formation of absolutely stable strange quark matter, a configuration of matter more stable than the most stable atomic nucleus, ^{62}Ni. Instead these objects should be named nucleon stars, since relatively isospin symmetric nuclear matter-in equilibrium with condensed K^- mesons-may prevail in their interiors [3], hyperon stars if hyperons (Σ,Λ,Ξ, possibly in equilibrium with the Δ resonance) become populated in addition to the nucleons, quark hybrid stars if the highly compressed matter in the centers of neutron stars were to transform into u, d, s quark matter, or strange stars if strange quark matter were to be more stable than nuclear matter. Of course, at present one does not know from experiment at what density the expected phase transition to quark matter occurs. Neither do lattice Quantum ChromoDynamical (QCD) simulations provide a conclusive guide yet. From simple geometrical considerations it follows that, for a characteristic nucleon radius of $r_N \sim 1$fm, nuclei begin to touch each other at densities of $\sim (4\pi r_N^3/3))^{-1} \approx 0.24$ fm^3, which is less than twice the baryon number density of ordinary nuclear matter, $\rho_0 = 0.16$ fm^3 (energy density $\epsilon_0 = 140$ MeV/fm^3). Depending on the rotational frequency and stellar mass, such densities are easily surpassed in the cores of neutron stars so gravity may have broken up the

neutrons (n) and protons (p) in the centers of neutron stars into their constituents. The phase diagram of quark matter, expected to be in a color superconducting phase, is very complex [3,4]. At asymptotic densities the ground state of QCD with a vanishing strange quark mass is the color-flavor locked (CFL) phase. This phase is electrically charge neutral without any need for electrons for a significant range of chemical potentials and strange quark masses.

An intriguing aspect of quantum mechanics is that even at absolute zero temperature quantum fluctuations prevail in a system, whereas all thermal fluctuations are frozen out. These quantum fluctuations are able to induce a macroscopic phase transition in the ground state of a many-body system, when the ratio of two competing terms in the underlying Hamiltonian is varied across a critical value [5]. The instability of the quantum critical behavior with respect to (w.r.t.) the disorder can be interpreted as a signal for phenomena of localization. One example is the strongly-interacting electron (non-Fermi) liquid with different strengths of disorder. Interesting issues are the quantum phase transition (QPT) and quantum critical point (QCP).

Quite recently McLaughlin *et al.* [6] searched for radio sources that vary on much shorter timescales. They found eleven objects characterized by single, dispersed bursts having durations between 2 and 30 ms. The average time intervals between bursts range from 4 min to 3 h with radio emission typically detectable for < 1 s per day. From an analysis of the burst arrival times, they have identified periodicities in the range 0.4-7 s for ten of the eleven sources, suggesting origins in rotating neutron stars. Meanwhile as all pulsars from which giant pulses have been detected appear to have high values of magnetic field strength at their light cylinder radii [7]. While the Crab pulsar has a magnetic field strength at the light cylinder of 9.3×10^5 G [6], this value ranges from only 3 to 30G for these sources, suggesting that the bursts originate from a different emission mechanism. They therefore concluded that these sources represent a previously unknown population of bursting neutron stars, which they call rotating radio transients (RRATs). These interesting new observations make us to investigate the rotation (e.g., it is still controversial how much angular momentum the iron cores have before the onset of the gravitational-collapse) [1,6] as well as Pauli-blocking effects [8] in compact stars considering the phase diagram [4].

In present approach the Uehling-Uhlenbeck collision term [9-10] which could describe the collision of a gas of dilute hard-sphere Fermi- or Bose-particles by tuning a parameter γ : a Pauli-blocking factor (or γf with f being a normalized (continuous) distribution function giving the number of particles per cell) is adopted together with a free-orientation θ (which is related to the relative direction of scattering of particles w.r.t. to the normal of the propagating plane-wave front) into the quantum discrete kinetic model [10] which can be used to obtain dispersion relations of plane (sound) waves propagating in different-statistic gases (of particles). We then study the critical behavior based on the acoustical analog [12] which has been verified before. The possible phase diagram (as the temperature is changed) related to the effective number of thermodynamic degrees of freedom (which is useful in QCD thermodynamics, it is one observable whose value changes by more than an order of magnitude across the crossover transition from hadron gas to quark-gluon plasma (QGP)[11]) we obtained resemble qualitatively those proposed before.

2 Theoretical Formulations

Within this presentation, we shall assume that the gas is composed of identical hard-sphere particles of the same mass [10]. (Note that most of the similar formulations could be traced in Chu [10] or [12-13]) The velocities of these particles are restricted to, e.g., : $\mathbf{u}_1, \mathbf{u}_2, \cdots, \mathbf{u}_p$, p is a finite positive integer. The discrete number densities of particles are denoted by $N_i(\mathbf{x}, t)$ associated with the velocities $\mathbf{u}_i$ at point $\mathbf{x}$ and time t. If only nonlinear binary collisions and the evolution of N_i are considered, we have

$$\frac{\partial N_i}{\partial t} + \mathbf{u}_i \cdot \nabla N_i = F_i \equiv \frac{1}{2} \sum_{j,k,l} (A_{kl}^{ij} N_k N_l - A_{ij}^{kl} N_i N_j), \quad i \in \Lambda = \{1, \cdots, p\}, \tag{1}$$

where (i, j) and (k, l) ($i \neq j$ or $k \neq l$) are admissible sets of collisions [10]. Here, the summation is taken over all $j, k, l \in \Lambda$, where A_{kl}^{ij} are nonnegative constants satisfying [10] $A_{kl}^{ji} = A_{kl}^{ij} = A_{lk}^{ij}$, $A_{kl}^{ij}(\mathbf{u}_i + \mathbf{u}_j - \mathbf{u}_k - \mathbf{u}_l) = 0$, and $A_{kl}^{ij} = A_{ij}^{kl}$. The conditions defined for the discrete velocities above require that there are elastic, binary collisions, such that momentum and energy are preserved, i.e., $\mathbf{u}_i + \mathbf{u}_j = \mathbf{u}_k + \mathbf{u}_l$, $|\mathbf{u}_i|^2 + |\mathbf{u}_j|^2 = |\mathbf{u}_k|^2 + |\mathbf{u}_l|^2$, are possible for $1 \leq i, j, k, l \leq p$. We note that, the summation of N_i ($\sum_i N_i$) : the total discrete number density here is related to the macroscopic density : $\rho\,(= m_p \sum_i N_i)$, where m_p is the mass of the particle [10].

Together with the introducing of the Uehling-Uhlenbeck collision term [10] : $F_i = \sum_{j,k,l} A_{kl}^{ij} [N_k N_l (1 + \gamma N_i)(1 + \gamma N_j) - N_i N_j (1 + \gamma N_k)(1 + \gamma N_l)]$, into equation (1), for $\gamma < 0$ (normally, $\gamma = -1$), we can then obtain a quantum discrete kinetic equation for a gas of Fermi-particles; while for $\gamma > 0$ (normally, $\gamma = 1$) we obtain one for a gas of Bose-particles, and for $\gamma = 0$ we recover the equation (1).

Considering binary collisions only, from equation above, the model of quantum discrete kinetic equation for Fermi or Bose gases proposed before is then a system of $2n(= p)$ semilinear partial differential equations of the hyperbolic type :

$$\frac{\partial}{\partial t} N_i + \mathbf{v}_i \cdot \frac{\partial}{\partial \mathbf{x}} N_i = \frac{cS}{n} \sum_{j=1}^{2n} N_j N_{j+n} (1 + \gamma N_{j+1})(1 + \gamma N_{j+n+1}) -$$

$$2cS N_i N_{i+n} (1 + \gamma N_{i+1})(1 + \gamma N_{i+n+1}), \qquad i = 1, \cdots, 2n, \tag{2}$$

where $N_i = N_{i+2n}$ are unknown functions, and $\mathbf{v}_i = c(\cos[\theta + (i-1)\pi/n], \sin[\theta + (i-1)\pi/n])$; c is a reference velocity modulus and the same order of magnitude as that used in Ref. 10 (c, the sound speed in the absence of scatters), θ is the orientation starting from the positive $x-$axis to the u_1 direction, S is an effective collision cross-section for the collision system.

Since passage of the plane (sound wave) will cause a small departure from an equilibrium state and result in energy loss owing to internal friction and heat conduction, we linearize above equations around a uniform equilibrium state (particles' number density : N_0) by setting $N_i(t, x) = N_0\,(1 + P_i(t, x))$, where P_i is a small perturbation. After some similar manipulations (please refer to Chu in [12-13]), with $B = \gamma N_0 < 0$, which gives or defines the (proportional) contribution from the Fermi gases (if $\gamma < 0$, e.g., $\gamma = -1$) or the Bose gases ($B > 0$, if $\gamma > 0$, e.g., $\gamma = 1$), we then have

$$[\frac{\partial^2}{\partial t^2} + c^2 \cos^2[\theta + \frac{(m-1)\pi}{n}] \frac{\partial^2}{\partial x^2} + 4cSN_0(1 + B)\frac{\partial}{\partial t}] D_m = \frac{4cSN_0(1 + B)}{n} \sum_{k=1}^{n} \frac{\partial}{\partial t} D_k, \tag{3}$$

where $D_m = (P_m + P_{m+n})/2$, $m = 1, \cdots, n$, since $D_1 = D_m$ for $1 = m$ (mod $2n$).
We are ready to look for the solutions in the form of plane wave $D_m = a_m \exp\, i(kx - \omega t)$, $(m = 1, \cdots, n)$, with $\omega = \omega(k)$. This is related to the dispersion relations of 1D (forced) plane wave propagation in Fermi or Bose gases. So we have

$$(1 + ih(1 + B) - 2\lambda^2 cos^2[\theta + \frac{(m-1)\pi}{n}])a_m - \frac{ih(1+B)}{n}\sum_{k=1}^{n} a_k = 0, \qquad m = 1, \cdots, n, \quad (4)$$

where

$$\lambda = kc/(\sqrt{2}\omega), \qquad\qquad h = 4cSN_0/\omega \qquad \propto \quad 1/K_n,$$

where h is the rarefaction parameter of the gas; K_n is the Knudsen number which is defined as the ratio of the mean free path of gases to the wave length of the plane (sound) wave.

3 Numerical Results and Discussions

We firstly introduce the concept of acoustical analog [12] in brief. In a mesoscopic system, where the sample size is smaller than the mean free path for an elastic scattering, it is satisfactory for a one-electron model to solve the time-independent Schrödinger equation : $-(\hbar^2/2m)\nabla^2\psi + V'(\vec{r})\psi = E\psi$ or (after dividing by $-\hbar^2/2m$) $\nabla^2\psi + [q^2 - V(\vec{r})]\psi = 0$, where q is an (energy) eigenvalue parameter, which for the quantum-mechanic system is $\sqrt{2mE/\hbar^2}$. Meanwhile, the equation for classical (scalar) waves is $\nabla^2\psi - (\partial^2\psi/c^2\,\partial t^2) = 0$ or (after applying a Fourier transform in time and contriving a system where c (the wave speed) varies with position $\vec{r}$) $\nabla^2\psi + [q^2 - V(\vec{r})]\psi = 0$, here, the eigenvalue parameter q is ω/c_0, where ω is a natural frequency and c_0 is a reference wave speed. Comparing the time dependencies one gets the quantum and classical relation $E = \hbar\omega$. The localized state could thus be determined via E or the rarefaction parameter (h) which is related to the ratio of the collision frequency and the wave frequency [12].
The complex spectra ($\lambda = \lambda_r +$ i λ_i; the real part $\lambda_r = k_r c/(\sqrt{2}\omega)$: sound dispersion, a relative measure of the sound or phase speed; the imaginary part $\lambda_i = k_i c/(\sqrt{2}\omega)$: sound attenuation or absorption) could be obtained from the complex polynomial equation above. Here, the Pauli-blocking parameter (B) could be related to the occupation number of different-statistic particles of gases [10]. To examine the critical region possibly tuned by the Pauli-blocking measure $B = \gamma N_0$ and the free orientation θ, as evidenced from previous Boltzmann results [12] (cf. Chu therein) : $\lambda_i = 0$ for cases of $\theta = \pi/4$ (or $B = -1$), we firstly check those spectra near $\theta = 0$, say, $\theta = 0.005$ and $\theta = \pi/4 \approx 0.7854$, say, $\theta = 0.78535$ for a B-sweep (B decreases from 1 to -1), respectively. Note that, as the free-orientation θ is not zero, there will be two kinds of propagation of the disturbance wave : sound and diffusion modes [13-14]. The latter (anomalous) mode has been reported in Boltzmann gases (cf. Ref. 12 by Chu) and is related to the propagation of entropy wave which is not used in the acoustical analog here. The absence of (further) diffusion (or maximum absorption) for the sound mode at certain state (h, corresponding to the inverse of energy E; cf. Chu in Ref. 12) is classified as a localized state (resonance occurs) based on the acoustical analog [12]. The state of decreasing h might, in one

case [15], correspond to that of T (absolute temperature) decreasing as the mean free path is increasing (density or pressure decreasing).

We have observed the max. λ_i (absorption of sound mode, relevant to the localization length according to the acoustical analog [12]) drop to around four orders of magnitude from $\theta = 0.005$ to 0.78535 (please see Chu (2001) in [12])! This is a clear demonstration of the effect of free orientations. Meanwhile, once the Pauli-blocking measure (B) increases or decreases from zero (Boltzmann gases), the latter (Fermi gases : $B < 0$) shows opposite trend compared to that of the former (Bose gases : $B > 0$) considering the shift of the max. λ_i state : δh. $\delta h > 0$ is for Fermi gases ($|B|$ increasing), and the reverse ($\delta h < 0$) is for Bose gases (B increasing)! This illustrates partly the interaction effect (through the Pauli exclusion principle). These results will be crucial for further obtaining the phase diagram (as the density or temperature is changed) tuned by both the free orientation and the interaction. Here, $B = -1$ or $\theta = 0, \pi/4$ might be fixed points.

To check what happens when the temperature is decreased (or h is decreased) to near $T = 0$ or $T = T_c$, we collect all the data based on the acoustical analog from the dispersion relations (especially the absorption of sound mode) we calculated for ranges in different degrees of the orientation (here, θ is up to $\pi/4$ considering single-particle scattering and binary collisions; in fact, effects of θ are symmetric w.r.t. $\theta = \pi/4$ for $0 \leq \theta \leq \pi/2$; cf. Chu (2001) in Ref. 12) and Pauli-blocking measure. After that, we plot the possible phase diagram for the inverse of the rarefaction parameter vs. the orientation (which is related to the scattering) into Fig. 1 (for different Bs : $B = -0.98, -0.9, -0.1, 0, 0.1, 1$). Here, the Knudsen number (K_n) $\propto$ MFP/λ_s with MFP and λ_s being the mean free path and wave length, respectively and the temperature vs. MFP relations could be, ine one case, traced from Ref. 15 (following Fig. 3 therein). This figure shows that as the temperature decreases to a rather low value, the orientation will decrease sharply (at least for either Bose or Fermi gases). There is no doubt that this result resembles qualitatively that proposed before [16] for cases of the pressure vs. temperature analogue.

On the other hand, qualitatively similar results (cf. Fig. 4 in [17] : theirin higher relative pressure corresponding to λ_r here) show that (i) once the orientation θ increases, for the same h (or temperature [15]), the dispersion λ_r (or the relative pressure [17]) increases (please refer to Chu (2001) in [12]); (ii) as $|B|$ (B: the Pauli-blocking parameter) increases, the dispersion (λ_r) will reach the continuum or hydrodynamical limit (larger h or high temperature regime) earlier. The phase speed of the plane (sound) wave in Bose gases (even for small but fixed h) increases more rapid than that of Fermi gases (w.r.t. to the higher temperature conditions : larger h) as the relevant parameter B increases. For all the rarefaction measure (h), perturbed plane waves propagate faster in Bose-particle gases than Boltzmann-particle and Fermi-particle gases (e.g., see [18] or [13]). In fact, the real part (λ_r) also resembles qualitatively those reported in [19] for $T > T_c$ cases.

As for the imaginary part (λ_i), there is the maximum absorption (or attenuation) for certain h (the rarefaction parameter) which resembles that reported in [20] (cf. Fig. 1 (b) therein). We observed a jump of the (relative) sound speed in the multiple scattering case (cf. Chu (2002) in [12]) which was also reported in [21](at the phase transition between hadronic phase and QGP). To know the detailed effects of interactions (tuned by the Pauli-blocking parameter : B here)

and the orientation, which could be linked to the effective number of thermodynamic degrees of freedom (as stated in [11] : ν, for an ideal gas of massless, non-interacting constituents, ν counts the number of bosonic degrees of freedom plus the number of fermionic degrees of freedom weighted by 7/8), we plot θ (of which the localization or resonance occurs for specific B) vs. T (the temperature, in arbitrary units) in Figs. 2 and 3 by referring to two possibly localized states ($\theta = 0$ or $\pi/4$; cf. Chu (2001) in [12]). The trends here resemble that of Fig. 1 in [11] once the effective number of thermodynamic degrees of freedom is proportional to the product of the orientation and the Pauli-blocking parameter ($\nu \propto \theta \times |B|$). Then there might be different behaviors separated by crossover regions as shown in Fig. 2. We remind the readers that for the case of $\theta = \pi/4$ dominated (Fig. 3), as the lower temperature is associated with the higher density, fermions ($B < 0$) link to the lower temperature regime (under the same orientation).

It is clear that depending on the temperature regime investigated, there would be different values of ν. If there are differences between ours and those in [11] (presumed that the matter under study is in (approximate) local thermal equilibrium. At RHIC, such evidence is believed to be provided by the agreement of the elliptic flow [22] measured in noncentral collisions with hydrodynamic model predictions. Such predictions are based on the assumption that the matter behaves like a fluid in local thermal equilibrium, with arbitrarily short mean free paths and correspondingly strong interactions.), one possible explanation could be that the assumption of a completely thermal medium is a simplification [23]. The acoustic perturbations we treated are close to the thermodynamic equilibrium (for Bose or Fermi gases). Other reasoning is related to the different types of particles (with or without fragmentation) being considered. One interesting observation is that the attenuation of jet (quenching) observed at RHIC resembles qualitatively the attenuation of plane (sound) waves (cf. Chu in [12]).

With above results, then our approach could provide an effective theory based on the opposite picture of very strong interaction (via the tuning of B and θ) and very small mean free paths (h is large) [24]. This can also be useful to the study of problems in astrophysics : like compact stars. For instance, one of the most striking features of QCD is asymptotic freedom: the force between quarks becomes arbitrarily weak as the characteristic momentum scale of their interaction grows larger. This immediately suggests that at sufficiently high densities and low temperatures (corresponding to the case of Fig. 3 here; cf. Chu (2001) in [12] since $\theta = \pi/4$ is also possible and thus dominates the localized behavior or transition) matter will consist of a Fermi sea of essentially free quarks, whose behavior is dominated by the freest of them all: the high-momentum quarks that live at the Fermi surface. If the strange matter hypothesis is true, a new class of compact stars called strange stars should exist. They would form a distinct and disconnected branch of compact stars and are not a part of the continuum of equilibrium configurations that include white dwarfs and neutron stars. In principle, strange and neutron stars could coexist.

To conclude in brief, our illustrations here, although are based on the acoustical analog of our quantum discrete kinetic calculations, can indeed show the Fermi and Bose liquid (say, Cooper pairs) and their critical behavior for the transition (at least valid to the regime $T > T_c$ considering the QGP) once the temperature is decreased to rather low values. We shall investigate more complicated problems in the future [24-26] (e.g., the saturated orientation shown in Fig. 3

which is almost the same for all different-statistic gases of particles might be relevant to the Stefan-Boltzmann limit; cf. Fig. 5 in [25] by Rischke).

References

[1] K. Kotake, K. Sato and K. Takahashi, Rep. Prog. Phys. **69**, 971 (2006).

[2] J.R. Oppenheimer and G.M. Volkoff, Phys. Rev. **55**, 374 (1939). R.C. Tolman, Phys. Rev. 55, 364 (1939).

[3] S.L. Shapiro and S.A. Teukolsky, *Black Holes, White Dwarfs and Neutron Stars: The Physics of Compact Objects* (Wiley, New York, 1983). F. Weber, Prog. Particle Nucl. Phys. **54**, 193 (2005). H. Heiselberg and V. Pandharipande, Annu. Rev. Nucl. Part. Sci. **50**, 481 (2000).

[4] M. Alford, Dense Quark Matter in Compact Stars, in : W. Plessas and L. Mathelitsch (Eds.), Lect. Notes Phys. **583**, pp. 81-115, (Springer, Berlin, 2002).

[5] L.D. Landau, Sov. Phys. JETP **5**, 101 (1957). C.M. Varma, Z. Nussinov, and W. van Saarloos, Phys. Rep. **361**, 267 (2002).

[6] M.A. McLaughlin, A. G. Lyne *et al.*, Nature **439**, 817 (2006).

[7] S. Johnston and R.W. Romani, Astrophys. J. **590**, L95 (2003).

[8] M.S. Hussein, R.A. Rego and C.A. Bertulani, Phys. Rep. **201**, 279 (1991). M.A.G. Alvarez, N. Alamanos, L.C. Chamon and M.S. Hussein, nucl-th/0501084.

[9] A. Dobado and F.J. Llanes-Estrada, Phys. Rev. D **69**, 116004 (2004). D.T. da Silva and D. Hadjimichef, J. Phys. G-Nucl. Part. Phys. **30**, 191 (2004).

[10] V.V. Vedenyapin, I.V. Mingalev and O.V. Mingalev, Russian Academy of Sciences Sbornik Mathematics **80** 271 (1995). A. K.-H. Chu, Phys. Scr. **69**, 170 (2004).

[11] B. Müller and K. Rajagopal, Eur. Phys. J. C **43**, 15 (2005).

[12] J.D. Maynard, Rev. Mod. Phys. **73**, 401 (2001). K.-H. W. Chu, J. Phys. A Math. and General **35**, 1919 (2002). K.-H. W. Chu, J. Phys. A Math. and General **34**, L673 (2001).

[13] R. K.-H. Chu, Meccanica **39**, 383 (2004). A. K.-H. Chu, cond-mat/0411627.

[14] R.J. Jr. Mason, in *Rarefied Gas Dynamics*, edited by J.H. de Leeuw (Academic Press, New York, 1965), vol. 1, p. 48.

[15] D. Einzel and J.M. Parpia, J. Low Temp. Phys. **109**, 1 (1997).

[16] G. Boyd *et al.*, Phys. Rev. Lett. **75**, 4169 (1995). M. Okamoto *et al.*, Phys. Rev. D **60**, 094510 (1999). M. Alford, Nucl. Phys. B (Proc. Suppl.) **117**, 65 (2003).

[17] F. Karsch, Nucl. Phys. A **698**, 199 (2002).

[18] K.-H. W. Chu, Preprint (2004).

[19] M. Asakawa and T. Hatsuda, Nucl. Phys. A **610**, 470 (1996).

[20] W. Broniowski and B. Hiller, Phys. Lett. B **392**, 267 (1997).

[21] Yu.A. Tarasov, Phys. Lett. B **379**, 279 (1996).

[22] P.F. Kolb, P. Huovinen, U. Heinz and H. Heiselberg, Phys. Lett. B **500**, 232 (2001). X.-N. Wang, Nucl. Phys. A **750**, 98 (2005).

[23] B. Müller, Nucl. Phys. A **750**, 84 (2005).

[24] E. Shuryak, Prog. Particle Nucl. Phys. **53**, 273 (2004). E. Shuryak, Nucl. Phys. A **750**, 64 (2005).

[25] D.H. Rischke, Prog. Particle Nucl. Phys. **52**, 197 (2004). T.K. Nayak, Pramana-J. Phys. **62**, 623 (2004).

[26] J. Liao and E.V. Shuryak, Phys. Rev. D **73**, 014509 (2006). M. Stephanov, Acta Physica Polonica B **35**, 2939 (2004). M. Gyulassy and L. McLerran, Nucl. Phys. A **750**, 30 (2005). M. Bluhm, B. Kämpfer and G. Soff, Phys. Lett. B **620**, 131 (2005).

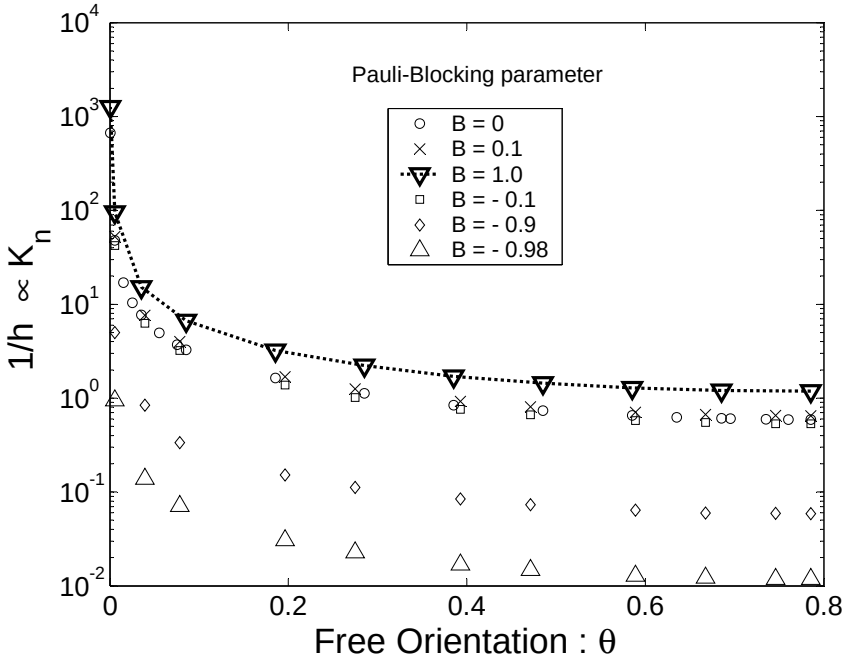

Fig. 1 Possible phase diagram for different-statistic gases w.r.t. the free orientation (θ) and Knudsen number ($K_n \propto$ the mean free path/wave length). $B > 0$: bosonic particles; $B < 0$: fermionic particles [10]. The orientation is related to the scattering. K_n might be transformed to the dimensionless or relative temperature (cf. Fig. 3 in [15]).

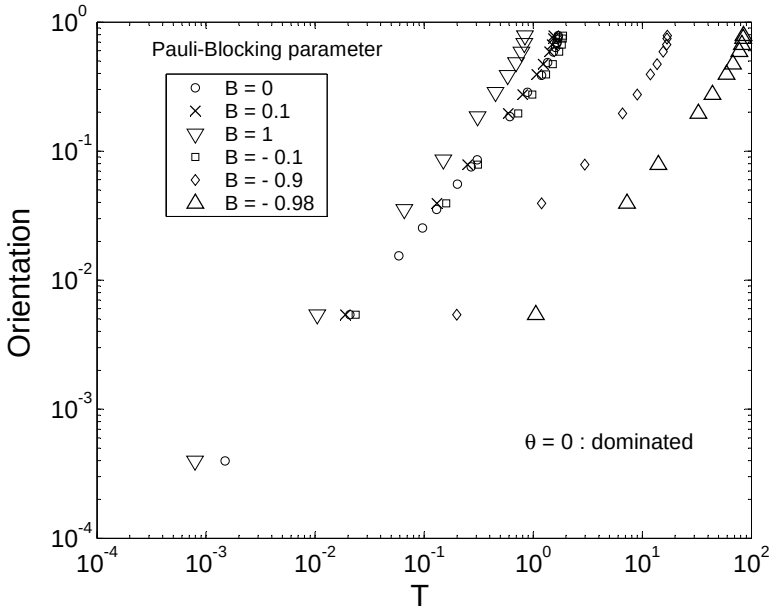

Fig. 2 Possible phase diagram for different-statistic gases w.r.t. the orientation (θ) and temperature $T \propto h$ (the rarefaction measure). The unit of T is arbitrary. $B > 0$: bosonic particles; $B < 0$: fermionic particles [10]. The trend here resembles that of Fig. 1 in [11] once ν (the effective number of thermodynamic degrees of freedom) is $\propto \theta \times |B|$.

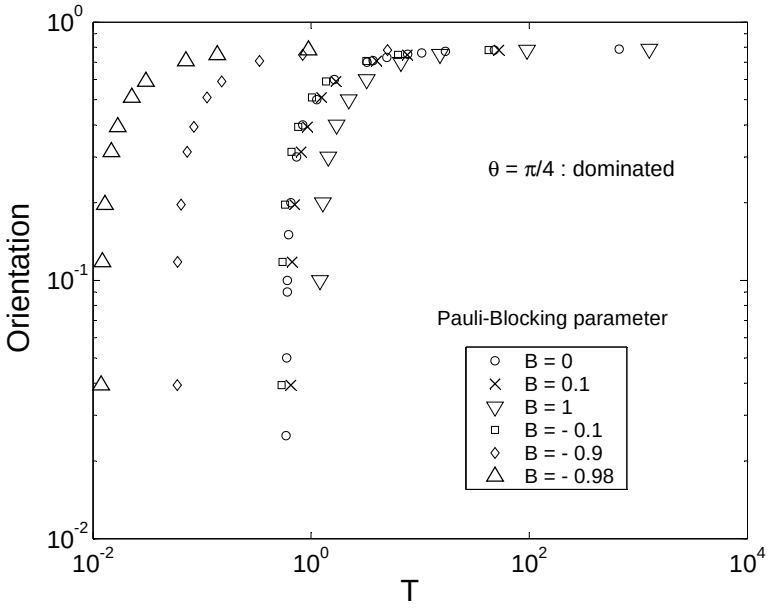

Fig. 3 Possible phase diagram for different-statistic gases w.r.t. the orientation and temperature $T \propto K_n$ (the Knudsen number). The unit of T is arbitrary (cf. Fig. 3 in [15]).